Magnetic Field Dependence of the Size Effect in the Transport Coefficients of a Cadmium Single Crystal at Liquid-Helium Temperatures*†

C. G. GRENIER, K. R. EFFERSON,‡ AND J. M. REYNOLDS
Department of Physics, Louisiana State University, Baton Rouge, Louisiana
(Received 13 August 1965)

Magnetomorphic oscillations periodic in the magnetic field have been observed in transverse magnetic fields in the transport coefficients of a cadmium single crystal at liquid-helium temperatures. The experimental coefficients in which magnetomorphic oscillations have been observed are: the transverse magnetoresistivity ρ_{11}, the Hall resistivity ρ_{21}, the transverse thermal magnetoresistivity γ_{11}, the Righi-Leduc resistivity γ_{21}, the adiabatic thermoelectric coefficient ϵ_{11}', and the adiabatic Nernst-Ettinghausen coefficient ϵ_{21}'. These oscillations have an average period of about 565 G for a sample thickness 1.02 mm and are believed to originate with the lens-shaped Fermi surface in the third Brillouin zone of cadmium. The theory of magnetomorphic oscillation for the case of free electrons is found to agree for the most part with the experimental results, except in the case of the oscillations in the quantity ϵ_{11}'' (thermoelectric coefficient), which have been found to be of an order of magnitude 20 times larger than predicted by the free-electron theory. The extension of the theory to the case of nonspherical Fermi surfaces, and to the case of lens-shaped Fermi surfaces in particular, fails to account for the anomaly in this coefficient. In addition to the oscillations of period 565 G, another set of oscillations of period 132 G was detected in the Hall effect. It is suggested that these short-period oscillations may be associated with the hole arms in the second Brillouin zone and are probably due to the truncation of the arm when it splits into its three branches.

INTRODUCTION

WHEN the dimensions of a metallic sample are of the order of the mean free path of the electrons, scattering at the boundaries must be taken into account when calculations of the transport effects are made. Effects in which boundary scattering cannot be neglected are known as morphic or size effects and the magnetic dependence of these size effects are known as magnetomorphic effects. This paper presents the results of measurements of magnetomorphic effects occurring in the transport coefficients of a cadmium single crystal. All measurements were made at liquid-helium temperatures in a transverse magnetic field (see Fig. 1). It was found that oscillations periodic in the magnetic field H exist in the transport coefficients of the cadmium crystal. These oscillations have been attributed to size effects.

Much of the work that has already been done on size effects corresponds either to the zero magnetic field case or the longitudinal magnetic field case[1] and little has been done in the case of transverse fields. Oscillations in the Hall effect and the transverse magnetoresistance were predicted by Sondheimer[2] and have been observed by several experimenters.[3–8] Oscillations are also expected in the transverse thermal magnetoresistance, the Righi-Leduc effect, the transverse thermoelectric effect, and the Nernst-Ettinghausen effect, as was shown by Blatt[9] who extended Sondheimer's theory to the case of thermal effects. To the authors' knowledge, magnetomorphic oscillations in these effects have not previously been observed.

Since the theories of Blatt and Sondheimer deal only

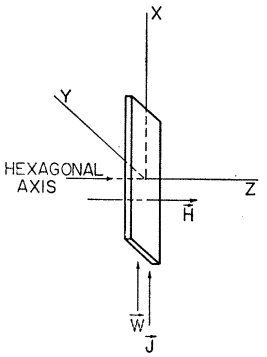

FIG. 1. Orientation of the crystal with respect to the magnetic field H, the electrical current **J**, and the heat current **W**. The hexagonal axis of the crystal is along the magnetic field.

* This work was done under the auspices of the U. S. Atomic Energy Commission and supported in part by the National Science Foundation for the use of the Computer Research Center.

† Part of this work was submitted (by K. E.) in partial fulfillment of the requirements for the Ph.D. at Louisiana State University.

‡ Present address: Oak Ridge National Laboratory, Oak Ridge, Tennessee.

[1] For example, size effects in longitudinal magnetic fields have been investigated by: B. N. Aleksandrov and M. I. Kaganov, Zh. Eksperim. i Teor. Fiz. **41**, 1333 (1961) [English transl.: Soviet Phys.—JETP **14**, 948 (1962)]; V. F. Gantmakher, Zh. Eksperim. i Teor. Fiz. **43**, 345 (1962) [English transl.: Soviet Phys.—JETP **16**, 247 (1963)]; M. Ya. Azbel and R. N. Gurzhi, Zh. Eksperim. i Teor. Fiz. **42**, 1632 (1962) [English transl.: Soviet Phys.—JETP **15**, 1133 (1962)]; B. N. Aleksandrov, Zh. Eksperim. i Teor. Fiz. **43**, 399 (1962) [English transl.: Soviet Phys.—JETP **16**, 286, 871 (1963)].

[2] E. H. Sondheimer, Phys. Rev. **80**, 401 (1950) and Advan. Phys. **1**, 1 (1952).

[3] J. Babiskin and P. H. Siebenmann, Phys. Rev. **107**, 1249 (1957).

[4] M. Yaqub and J. F. Cochran, Phys. Rev. Letters **10**, 370 (1963); Phys. Rev. **137**, A1182 (1965).

[5] N. H. Zebouni, R. E. Hamburg, and H. J. Mackey, Phys. Rev. Letters **11**, 260 (1963).

[6] J. M. Reynolds, K. R. Efferson, C. G. Grenier, and N. H. Zebouni, *Proceedings of Ninth International Conference on Low Temperature Physics, Ohio State University, 1964* (Plenum Press, Inc., New York, 1965), p. 808.

[7] J. A. Munarin and J. A. Marcus, *Proceedings of Ninth International Conference on Low Temperature Physics, Ohio State University, 1964* (Plenum Press, Inc., New York, 1965), p. 743.

[8] K. R. Efferson, C. G. Grenier, and J. M. Reynolds, Bull. Am. Phys. Soc. **10**, 126 (1965).

[9] F. J. Blatt, Phys. Rev. **95**, 13 (1954).

with spherical Fermi surfaces, an extension has been made to more general cases. The theory has been developed to include asymptotic high-field effects for Fermi surfaces which have rotational symmetry about the z axis, the z axis being parallel to the magnetic-field direction. The extended theory reduces to the asymptotic form of Blatt's theory for the case of free electrons.

Notation for the transport effects will be the same as that used by Grenier, Reynolds and Zebouni[10] where the kinetic transport equations are given by

$$\mathbf{J}=\hat{\sigma}\mathbf{E}^*-\hat{\epsilon}''\mathbf{G}$$
$$\mathbf{W}^*=-\hat{\pi}''\mathbf{E}^*+\hat{\lambda}''\mathbf{G}, \quad (1)$$

where the fluxes $\mathbf{J}$ (current density) and $\mathbf{W}^*$ (heat current density) are given as linear combinations of the affinities $\mathbf{G}$ (negative of the temperature gradient, $-\nabla T$) and $\mathbf{E}^*$ [electrical affinity; see Eq. (9c)]. These equations can be expressed in two alternative forms which are useful for expressing experimental results.

$$\mathbf{E}^*=\hat{\rho}\mathbf{J}+\hat{\epsilon}\mathbf{G} \qquad \mathbf{W}^*=-\hat{\pi}\mathbf{J}+\hat{\lambda}\mathbf{G}, \quad (2a)$$
$$\mathbf{E}^*=\hat{\rho}'\mathbf{J}+\hat{\epsilon}'\mathbf{W}^* \qquad \mathbf{G}=\hat{\pi}'\mathbf{J}+\hat{\gamma}\mathbf{W}^*. \quad (2b)$$

For the geometry used in this experiment (see Fig. 1), i.e., the magnetic field in the direction of the sixfold axis of symmetry and the effects measured in the basal plane, all the tensors in Eqs. (1) and (2) reduce to 2×2. By letting $\hat{a}$ be one of the tensors and by using Onsager's reciprocal relations, it can be shown that the tensors are all characterized by $a_{11}=a_{22}$ and $a_{21}=-a_{12}$. By defining $\hat{a}=a_{11}+ia_{12}$, it can be shown that the tensors $\hat{a}$ are homomorphic with the complex numbers a. (Note: The complex notation used is chosen to give agreement with that used by Blatt and Sondheimer.) This allows the tensors to be manipulated like complex numbers; for example, from Eqs. (1) and (2a) with the temperature gradient $-\mathbf{G}=0$, one obtains $\hat{\sigma}=\hat{\rho}^{-1}$ or $(\sigma_{11}+i\sigma_{12})=(\rho_{11}+i\rho_{12})^{-1}$. The tensor elements of $\hat{\sigma}$ are then easily obtained from the complex notation, i.e., $\sigma_{11}=\rho_{11}/(\rho_{11}^2+\rho_{12}^2)$ and $\sigma_{12}=-\rho_{12}/(\rho_{11}^2+\rho_{12}^2)$. Manipulation of Eqs. (1) and (2) yields, among other things, the following set of results which are used in this paper:

$$\hat{\sigma}=\hat{\rho}^{-1}, \quad (3a)$$
$$\hat{\lambda}=\hat{\gamma}^{-1}, \quad (3b)$$
$$\hat{\epsilon}''=\hat{\sigma}\hat{\lambda}\hat{\epsilon}'=\hat{\sigma}\hat{\epsilon}, \quad (3c)$$
$$\hat{\lambda}''=\hat{\lambda}+\hat{\epsilon}\hat{\pi}''. \quad (3d)$$

From Eq. (3a) it is seen that the kinetic coefficient $\hat{\sigma}$ can be determined directly from the experimental quantity $\hat{\rho}$. Equations (3b) and (3d) show that, if $\hat{\epsilon}\hat{\pi}''\ll\hat{\lambda}$ (which is usually the case at low temperatures), then $\hat{\lambda}''\approx\hat{\lambda}=\hat{\gamma}^{-1}$. Thus it is seen by Eqs. (3) that the kinetic coefficients $\hat{\sigma}$, $\hat{\lambda}$ and $\hat{\epsilon}''$ can be determined from the experimental quantities $\hat{\rho}$, $\hat{\gamma}$, and $\hat{\epsilon}'$. In measuring these quantities, it was found that all the following effects contained magnetomorphic oscillations periodic in H: ρ_{21} (Hall resistivity), ρ_{11} (transverse magnetoresistivity), γ_{11} (transverse thermal magnetoresistivity), γ_{21} (Righi-Leduc resistivity), ϵ_{11}' (adiabatic thermoelectric coefficient), ϵ_{21}' (adiabatic Ettinghausen-Nernst coefficient). The Onsager relation $\hat{\pi}''=T\hat{\epsilon}''$ makes unnecessary the determination of $\hat{\pi}'$, the experimental adiabatic Peltier coefficient, and if necessary allows the determination of the corrective terms $\hat{\epsilon}\hat{\pi}''$ in Eq. (3d).

CRYSTAL

The monocrystal on which the measurements were made was spark-cut and spark-planed from a bar of zone-refined cadmium.[11] After a slight acid polishing the crystal had the shape of a slab of diminsions $1.8\times0.556\times0.103_5$ cm at room temperature. The sample size at the liquid-He^4 temperature can readily be obtained. For example, the thickness $a=0.102$ cm will be used in further computation; it takes into account the c-axis contraction ratio 5.531/5.6167, which is the same reduction factor used by Daniel and MacKinnon.[12]

In addition to the quoted purity[11] of 99.9999%, other indications of purity are the facts that the resistance ratio of the crystal is $\rho_{300}/\rho_{4,2}=35\,000$ and that the electron mean free path is of the order of millimeters at liquid-helium temperatures.

The crystal was oriented (see Fig. 1) such that the x or 1 direction was along the length of the sample, the y or 2 direction was across the width of the sample and the z or 3 direction was perpendicular to the face of the slab and parallel to the hexagonal axis. The 1 and 2 directions are off by 12° from the binary and bisectrix axis, respectively. The magnetic field was applied in the z direction while the primary fluxes, i.e., the heat current density $\mathbf{W}^*$ and the current density $\mathbf{J}$, were applied in the x direction. Figure 1 shows the orientation of the magnetic field and the primary fluxes.

FREE-ELECTRON THEORY

For the orientation of the crystal shown in Fig. 1, the fields and temperature gradients are given by

$$\mathbf{H}=(0,0,H), \quad \mathbf{E}=(E_x,E_y,0),$$
$$\mathbf{G}=-\nabla T=(-\partial T/\partial x, -\partial T/\partial y, 0).$$

Assuming a relaxation time τ, Blatt[9] solves the steady-state Boltzmann equation [Eq. (4)] for the electronic distribution function, for the case of free electrons scattered diffusely at the surface of the sample,

$$\mathbf{v}\cdot\nabla_r f-e[\mathbf{E}+(1/c)\mathbf{v}\times\mathbf{H}]\cdot\nabla_p f=-(\partial f/\partial t)_{\text{coll}}. \quad (4)$$

[10] C. G. Grenier, J. M. Reynolds, and N. H. Zebouni, Phys. Rev. **129**, 1088 (1962).

[11] The bar of cadmium was obtained from Cominco Products, Incorporated and the spark cutter from Metal Research Limited, Cambridge, England.

[12] M. R. Daniel and L. MacKinnon, Phil. Mag. **8**, 537 (1963).

He then obtains expressions for the current density **J** and the heat current density **W**. His results can then be expressed in terms of the kinetic coefficients $\hat{\sigma}$, $\hat{\lambda}''$, and $\hat{\epsilon}''$ which were defined in the introduction. Under the simplifying assumption that τ is independent of the energy $\mathcal{E}$, the equations are

$$\hat{\sigma}_0=\sigma_{11_0}+i\sigma_{12_0}=\hat{\sigma}_{b0}\int_1^\infty (\tfrac{3}{2})(t^{-2}-t^{-4}) \times\{1+(st)^{-1}[\exp(-st)-1]\}dt, \quad (5a)$$

$$\hat{\lambda}_0=\lambda_{11_0}+i\lambda_{12_0}\simeq\hat{\lambda}_0''=\hat{\lambda}_{b0}''\int_1^\infty (\tfrac{3}{2})(t^{-2}-t^{-4}) \times\{1+(st)^{-1}[\exp(-st)-1]\}dt, \quad (5b)$$

$$\hat{\epsilon}_0''=\epsilon_{11_0}''+i\epsilon_{12_0}''=\hat{\epsilon}_{b0}''\int_1^\infty t^{-2} \times\{1+(st)^{-1}[\exp(-st)-1]\}dt, \quad (5c)$$

where the bulk effects (index b) are given by

$$\hat{\sigma}_{b0}=(e^2\tau'/m_0)N_0, \quad (6a)$$

$$\hat{\lambda}_{b0}''=L_nT(e^2\tau'/m_0)N_0, \quad (6b)$$

$$\hat{\epsilon}_{b0}''=(\pi^2k^2T/3e)(e^2\tau'/m_0)Z_0. \quad (6c)$$

The notation used is essentially that of Blatt and Sondheimer where applicable, i.e., $s=K_0+i\beta_0=(a/\Lambda)+i(a/r_0)$ where a is the thickness of the slab, Λ is the bulk mean free path of the electrons and $r_0=(m_0v_fc/eH)$ is the cyclotron radius; $t=v_f/v_z$ is the parameter of integration with v_f the Fermi velocity and v_z the velocity component in the z direction; $1/\tau'=(1/\tau_b)+i(eH/m_0c)$ where τ_b is the bulk time of relaxation; N_0 is the number of electrons per unit volume, Z_0 is the electronic density of states and L_nT is the free electron Wiedemann-Franz ratio. The subscript (0) stands for the case of free electrons. All other quantities are assumed to be expressed in standard notation.

The Formulation of the Asymptotic Oscillatory Effect

If an expansion of Eqs. (5a), (5b), and (5c) is made using the method of integration by parts, then for high-field behavior, i.e., $|s|\gg1$ and $\beta_0\gg K$,[13] it is found that a good approximation to the results can be obtained by taking only the first term of the expansion. Retaining only the oscillatory part, the transport coefficients are given by

$$\tilde{\sigma}_{11_0}+i\tilde{\sigma}_{12_0}=(-3\sigma_{12_{b0}}\beta_0^{-3}e^{-K}) \times[\cos\beta_0+i\cos(\beta_0+\pi/2)], \quad (7a)$$

$$\tilde{\lambda}_{11_0}+i\tilde{\lambda}_{12_0}=L_nTe^{(K-K')}(\tilde{\sigma}_{11}+i\tilde{\sigma}_{12}), \quad (7b)$$

$$\tilde{\epsilon}_{11_0}''+i\tilde{\epsilon}_{12_0}''=(-\epsilon_{12_{b0}}''\beta_0^{-2}e^{-K''}) \times[\cos(\beta_0-\pi/2)+i\cos\beta_0], \quad (7c)$$

where $\sigma_{12_{b0}}$ and $\epsilon_{12_{b0}}''$ have their asymptotic values $\sigma_{12_{b0}}=-(N_0ec)/H$, and $\epsilon_{12_{b0}}''=-(\pi^2k^2TcZ_0/3H)$. Different K, K', and K'' have been used to take account of possible different mean free paths for electronic and thermal effects. Equations (7) are valid also in the case where τ_b is energy-dependent.

Equations (7a), (7b), and (7c) are the expressions needed to compare free electron theory to experiment.

The Expected Oscillatory Behavior in the Free-Electron Case

The free-electron sphere in cadmium has the following characteristics[12]: radius $\hbar^{-1}R_f=1.41$ Å^{-1}, Fermi energy 7.73 eV, Fermi velocity 1.63×10^8 cm/sec. When Eqs. (7) are used the asymptotic free electron theory predicts the following results for periods, phases, and amplitudes of the oscillations.

Period

All the effects should have the same period. Since $\beta_0=a/r_0=2\pi H/P_0$, it is found that $P_0=(2\pi c/ae)R_f$, where $R_f=m_0v_f$ is the radius of the Fermi sphere. Using the value of $\hbar^{-1}R_f=1.41$ Å^{-1} for the radius of the free-electron sphere, the free-electron period should be $P_0=572G$ if the apparent thickness of the crystal corrected for temperature contraction is used in the computation (i.e., 1.02 mm).

Phase

(a) The coefficients $\tilde{\sigma}_{11}$, $\tilde{\lambda}_{11}$ and $\tilde{\epsilon}_{12}''$ are all in phase, with field values for the maxima occurring at integral values of the period P_0, i.e., $H_{\max}=nP_0$ where n is an integer.

(b) The coefficients $\tilde{\sigma}_{12}$ and $\tilde{\lambda}_{12}$ are in phase with the positions of maxima given by $H_{\max}=(n\pm1/4)P_0$ where the minus sign refers to electrons and the plus to holes. Note that for electrons these two coefficients should lag in phase by $\frac{1}{2}\pi$ as compared with the $\tilde{\sigma}_{11}$, $\tilde{\lambda}_{11}$, and $\tilde{\epsilon}_{12}''$ coefficients. Opposite results are expected for the $\tilde{\epsilon}_{11}''$ coefficient, with $H_{\max}=(n\mp1/4)P_0$.

Amplitudes

(a) Equality of amplitudes should hold between the real and imaginary parts of each of the complex terms in Eqs. (7), i.e., $|\tilde{\sigma}_{11}|=|\tilde{\sigma}_{12}|$, $|\tilde{\lambda}_{11}|=|\tilde{\lambda}_{12}|$, $|\tilde{\epsilon}_{11}''|=|\tilde{\epsilon}_{12}''|$.

(b) For low temperatures $e^{-K}\simeq e^{-K'}$ so that the Wiedemann-Franz law should hold, i.e., $|\tilde{\lambda}|=L_nT|\tilde{\sigma}|$.

(c) $|\tilde{\sigma}_{11}|$, $|\tilde{\sigma}_{12}|$, $|\tilde{\lambda}_{11}|$ and $|\tilde{\lambda}_{12}|$ should fall off with the fourth power of H, i.e., $|\tilde{\sigma}_{11}|\sim H^{-4}$, etc., while $|\tilde{\epsilon}_{12}''|$ and $|\tilde{\epsilon}_{11}''|$ should fall off as H^{-3}.

[13] This asymptotic condition is incompatible with the condition $\omega_c\tau\ll1$ of rigorous applicability of the transport Eq. (5), but it will be supposed this last condition of applicability is not too stringent. (ω_c is the cyclotron frequency.)

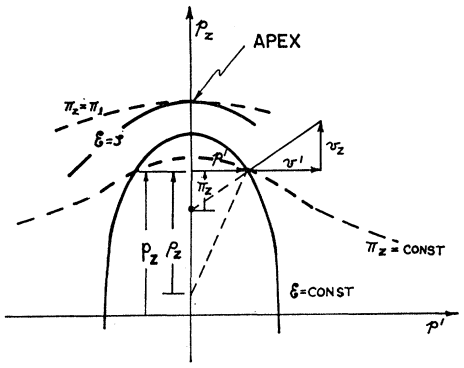

FIG. 2. Schematic representation of surfaces of constant energy $\mathcal{E}$ for axial symmetry, shown by the sections $\mathcal{E}(p_z,p')$=constant. The figure shows how the value of π_z is determined from the intercept of the normal to the surface of constant energy with the p_z axis. Surfaces of constant π_z are also indicated in broken lines by the sections π_z=constant. The figure shows how the value of ρ_z is determined from the intercept of the normal to the surface of constant π_z with the p_z axis.

(d) Calculation for $K=0$ of the free electron amplitudes gives $H^4|2\tilde{\sigma}_{12}|=6.86\times10^{18}G^4$ $(\Omega\ \text{cm})^{-1}$ and $H^3|2\tilde{\epsilon}_{11}''|=1.22T\times10^8G^3A$ cm^{-1} $(°\text{K})^{-1}$. The first of these values is represented by the letter F in Figs. 13, 14, and 18.

Some of the results required that a more general case be considered. Therefore, the theory is herein extended to include nonspherical Fermi surfaces which have rotational symmetry about the z axis.

THEORY FOR FERMI SURFACES WITH AXIAL SYMMETRY

The magnetic field and the direction of the axial symmetry are in the z direction. The Boltzmann equation, Eq. (4), is approached in the same manner as for the case of free electrons. With a trial solution of the form $f=f_0+f_1$ where $f_1=(c_1p_x+c_2p_y)\partial f_0/\partial\mathcal{E}$, Eqs. (4) become

$$v_xP_x+v_yP_y+(eH/c)(v_xc_2-v_yc_1)+p_x[c_1/\tau+v_z(\partial c_1/\partial z)]+p_y[c_2/\tau+v_z(\partial c_2/\partial z)]=0, \quad (8)$$

where

$$P_x=-eE_x^*+G_x(\partial\zeta/\partial T), \quad (9a)$$

$$P_y=-eE_y^*+G_y(\partial\zeta/\partial T), \quad (9b)$$

$$-eE_x^*=-eE_x+G_x(\partial\zeta/\partial T), \quad (9c)$$

$$-eE_y^*=-eE_y+G_y(\partial\zeta/\partial T), \quad (9d)$$

with ζ the chemical potential. Define $\mathbf{P}=P_x-iP_y$, $\mathbf{g}=c_1-ic_2$, $\mathbf{v}'=v_x-iv_y$, and $\mathbf{p}'=p_x-ip_y$ and note that $\mathbf{v}'/\mathbf{p}'=\mathbf{v}'^*/\mathbf{p}'^*=|\mathbf{v}'|/|\mathbf{p}'|=v_z/\pi_z$ for z the direction of axial symmetry (see Fig. 2 for the geometrical definition of π_z). The differential equation

$$\frac{\partial\mathbf{g}}{\partial z}+\left(\frac{1}{\tau v_z}+\frac{ieaH}{c\pi_z}\right)\mathbf{g}+\frac{\mathbf{P}}{\pi_z}=0, \quad (10)$$

is obtained, which has the solution

$$\mathbf{g}=-\pi_z^{-1}(s_z/a)^{-1}\mathbf{P}[1+F(\mathbf{p})\exp(-s_zz/a)], \quad (11)$$

where $F(\mathbf{p})$ is determined by the boundary condition $f=f_0$ for electrons scattered diffusely at the surface. It is seen that

$$F(\mathbf{p})=-1 \quad \text{for} \quad v_z>0$$
$$F(\mathbf{p})=-\exp s_z \quad \text{for} \quad v_z<0,$$

where

$$s_z=K+i\beta=\frac{a}{\tau v_z}+\frac{ieaH}{c\pi_z}=\frac{a}{\tau' v_z}.$$

Defining a complex current $\mathbf{J}=j_x-ij_y$ and remembering that f_0 does not contribute to the current integral, one obtains

$$\mathbf{J}=\frac{-2e}{h^3a}\int_0^a\int_{\mathbf{p}}\mathbf{v}'f dz d\mathbf{p}$$
$$=\frac{-2e}{h^3a}\int_0^a\mathbf{v}'\,\text{Re}(\mathbf{p}'^*\mathbf{g})\frac{\partial f_0}{\partial\mathcal{E}}dz d\mathbf{p}. \quad (12)$$

Let $d\mathbf{p}=|\mathbf{p}'|dp'dp_zd\psi$, integrate over z and ψ and retain only the oscillatory term, the result is

$$\tilde{\mathbf{J}}=(\tilde{\sigma}_{11}+i\tilde{\sigma}_{12})\mathbf{E}^*-(\tilde{\epsilon}_{11}''+i\tilde{\epsilon}_{12}'')\mathbf{G},$$

where

$$\tilde{\sigma}_{11}+i\tilde{\sigma}_{12}=-\frac{4a\pi e^2}{h^3}\int_{p'}\int_{p_z>0}\frac{v_z}{\pi_z}|p'|^3\frac{e^{-s_z}}{s_z^2}\frac{\partial f_0}{\partial\mathcal{E}}dp'dp_z, \quad (13a)$$

and

$$\tilde{\epsilon}_{11}''+i\tilde{\epsilon}_{12}''=-\frac{4a\pi e}{h^3}\int_{p'}\int_{p_z>0}\frac{v_z}{\pi_z}|p'|^3\times\left(\frac{\mathcal{E}-\zeta}{T}\right)\frac{e^{-s_z}}{s_z^2}\frac{\partial f_0}{\partial\mathcal{E}}dp'dp_z. \quad (13b)$$

Consider now a simple lens-shaped Fermi surface for which the transformation of Eqs. (13a) and (13b) by $p'=p'(\mathcal{E},\pi_z)$, $p_z=p_z(\mathcal{E},\pi_z)$ is unique for $p_z>0$. By making this transformation, defining ρ_z by

$$\frac{p'}{\rho_z}=\frac{\partial\pi_z}{\partial p'}\Big/\frac{\partial\pi_z}{\partial p_z}, \quad (14)$$

and integrating the new expression for Eq. (13a) over the energy $\mathcal{E}$, one obtains

$$\tilde{\sigma}_{11}+i\tilde{\sigma}_{12}=\frac{4a\pi e^2}{h^3}\int_{\pi_z>0}\frac{|p'|^2}{\pi_z}\frac{e^{-s_z}}{s_z^2}\left(\frac{\partial\pi_z}{\partial p_z}\right)^{-1}\times\left(\frac{1}{\pi_z}-\frac{1}{\rho_z}\right)^{-1}d\pi_z, \quad (15)$$

where all quantities now refer to their values for $\mathcal{E}=\zeta$, i.e., to their values on the Fermi surface. Note that (see Fig. 2) ρ_z is related to curves of constant π_z in the same manner as π_z is related to curves of constant $\mathcal{E}$. Although the derivation will be completed only for the case of the simple lens, the same procedures are applicable to other simple-shaped Fermi surfaces. An alternative form of Eq. (15) can be obtained by defining $t=\pi_l/\pi_z$ and $S_z=\pi p'^2$, where t is now the parameter of integration and S_z is the cross sectional area of the Fermi surface at some fixed value of p_z. The quantity π_l is an arbitrary value of π_z which in the case of the simple lens, is chosen to be the value of π_z at the apex of the lens, i.e., the radius of curvature of the lens at the apex. Equation (15) is now

$$\tilde{\sigma}_{11}+i\tilde{\sigma}_{12}=\frac{4ae^2}{h^3}\int_{t=1}^{\infty} S_z\frac{e^{-s_z}}{{s_z}^2}\left(\frac{1}{\pi_z}-\frac{1}{\rho_z}\right)^{-1}\left(\frac{\partial\pi_z}{\partial p_z}\right)^{-1}\frac{dt}{\pi_l}. \quad (16)$$

The Asymptotic Oscillatory Behavior Formulation

Since Eq. (16) has the form

$$\tilde{\sigma}_{11}+i\tilde{\sigma}_{12}=\int_1^{\infty} U(t)e^{-i\beta_l t}dt,$$

it can be expanded under the asymptotic condition $\beta_l=eaH/c\pi_l\gg 1$ by the method of integration by parts to obtain

$$\tilde{\sigma}_{11}+i\tilde{\sigma}_{12}=\left(\frac{c}{eaH}\right)^4\frac{8\pi e^2 a}{h^3}\pi_l{}^6\left(\frac{\rho_l}{\rho_l-\pi_l}\right)^2\left(\frac{\partial\pi_z}{\partial p_z}\right)^{-2}e^{-(K+i\beta_l)}, \quad (17)$$

where only the first term of the expansion has been retained. The radius of curvature of the surface $\pi_z=\pi_l$ at the point it touches the apex of the lens (see Fig. 2) is given by ρ_l. The case of free electrons is obtained by letting $\pi_z=p_z$, and $\pi_l=R_f$, where R_f is the radius of the Fermi sphere. It can be shown that the surfaces of constant π_z are planes for the case of free electrons, thus $\rho_l=\infty$. Substituting these quentities into Eq. (17) yields:

$$\tilde{\sigma}_{11_0}+i\tilde{\sigma}_{12_0}=(c/eaH)^4(8\pi e^2 a/h^3)R_f{}^6e^{-(K+i\beta_0)}, \quad (18)$$

which, since $R_f=3N_0h^3/8\pi$ and $\beta_l=aeH/m^*vc=aeH/R_fc$, is identical with the asymptotic Eq. (7a) obtained from Sondheimer's theory. Thus the amplitude of the oscillation associated with an apex, as compared to the free-electron case, is

$$|\tilde{\sigma}|/|\tilde{\sigma}_0|=r^6(1-\nu)^{-2}(\partial\pi_z/\partial p_z)^{-2}{}_{\pi_z=\pi_l}, \quad (19)$$

where $r=\pi_l/R_f$; $\nu=\pi_l/\rho_l$.

Similar treatment of Eq. (10b) for $\tilde{\epsilon}''$ gives

$$|\tilde{\epsilon}''|/|\tilde{\epsilon}_0''|=(m^*/m_0)r^3(1-\nu)^{-2}(\partial\pi_z/\partial p_z)^{-1}, \quad (20)$$

where m^* is the cyclotron mass at the apex and m_0 is the mass of a free electron. Equations (19) and (20) are generally true even with τ_b, π_z and m^* being smooth functions of $\mathcal{E}$ and p_z. Extension of the theory to the study of the heat flow and the determination of $\hat{\lambda}''$ leads to a result in $\tilde{\lambda}_{11}''+i\tilde{\lambda}_{12}''$ similar to those in $\hat{\sigma}$ in Eq. (19).

Thus it is seen that the case of nonspherical Fermi surfaces can be solved if the surfaces of constant $\mathcal{E}$ and surfaces of constant π_z are known, and that an asymptotic solution is readily obtained for the case of the lens-shaped surface. Extension to other simple Fermi surfaces with rotational symmetry about the z axis is only a matter of mechanics. More specifically, morphic oscillations should appear for any extremal values of π_z (or m^*v_z or $\partial S_z/\partial p_z$). This includes not only an apex but also cases for which π_z reaches a maximum or minimum, such as inflection zones occurring between the neck and belly of some Fermi surfaces. For those Fermi surfaces with inflection zones, $|\tilde{\sigma}_{12}|$ would follow an $H^{-7/2}$ law rather than the H^{-4} law found to hold in the case of the apex. Discontinuous or truncated Fermi surfaces would give $|\tilde{\sigma}_{12}|$ following an H^{-3} law, while "monochromatic" Fermi surfaces, i.e., those for which $\partial S_z/\partial p_z$ becomes independent of p_z over a finite range of p_z, would exhibit an H^{-2} law.

Equations (19) and (20) are the results needed to compare the theory of a lens to that of the free electron.

Expected Results in the Case of a Lens-Shaped Fermi Surface

To be more specific, cadmium has an electron lens-shaped Fermi surface in the third zone, the mapping of which apparently follows well the theoretical formulations given by Ziman.[14] Using the experimentally determined[12] principal axis radial values of the lens $\hbar^{-1}p_1\approx\hbar^{-1}p_2\approx 0.725$ Å^{-1}, $\hbar^{-1}p_3\approx 0.25$ Å^{-1} and Ziman's lens formula, the following parameters are obtained for this lens: energy gap $\Delta=0.91$ eV; Fermi energy $=7.47$ eV; len's apex radius of curvature $\hbar^{-1}\pi_l=(\hbar^{-1}/2\pi)(\partial S_z/\partial p_z)=1.36_3$ Å^{-1}, i.e., $r=\pi_l/R_f=0.96_7$; cyclotron mass $m^*=m_0$; Fermi velocity at the apex 1.57_4 10^8 cm/sec; the surfaces of constant π_z are planes $(\partial\pi_z/\partial\mathcal{E}=0)$ i.e., $\rho_z=\infty$ and $\nu=0$, $\partial\pi_z/\partial p_z=1.18$ at the lens apex; the amplitude factor for morphic conductivity oscillations $r^6(1-\nu)^{-2}(\partial\pi_z/\partial p_z)^{-2}=0.58$; the amplitude factor for morphic thermoelectric oscillations

$$r^3(1-\nu)^{-2}(\partial\pi_z/\partial p_z)^{-1}(m^*/m_0)=0.76.$$

Period

The period will depend on the radius of curvature of the lens at the apex, i.e., $P=(2\pi c/ae)\pi_l$ where π_l is the radius of curvature at the apex. If the Ziman's lens model is used, the expected period will be $P=553$ G, for a sample thickness of 1.02 mm.

---

[14] M. Ziman, *Electrons and Phonons* (Oxford University Press, London, 1960), p. 100.

Phase and Amplitudes

The relative phases and general considerations about the comparative amplitudes between the different effects are the same as that for the free electron case. Examination of Eq. (19) and Eq. (20) shows that $|\tilde{\sigma}|$ and $|\tilde{\epsilon}''|$ should not differ appreciably from the free-electron values as long as the apex characteristic parameters π_l, $\partial\pi_z/\partial p_z$, ν, m^* do not differ widely from those of the free-electron sphere. More specifically, if the lens model formulated by Ziman is used, with e^{-K} supposed equal to unity, then the following amplitudes are expected:

$$H^4|2\tilde{\sigma}_{12}| = 4.0\times10^{18}\Omega^{-1}\ \mathrm{cm}^{-1}\mathrm{G}^4$$

and

$$H^3|2\tilde{\epsilon}_{12}''| = 0.93T\times10^8\ \mathrm{A(^\circ K)^{-1}}.$$

The first of these values is indicated by the letter L on Figs. 13, 14, and 18.

EXPERIMENTAL RESULTS

A complete set of results has been obtained for the elements of the tensors $\hat{\rho}$, $\hat{\gamma}$, and $\hat{\epsilon}'$ at four temperatures: 4.0, 2.8, 2.0, and 1.6°K. During the course of these experiments, two distinct sets of oscillations were observed, both of which are periodic in the field H. One set, which will be referred to as long period or main oscillations, has a period of 564±3 G and has been observed in all the measured effects under appropriate conditions of temperature, magnetic field, and primary flux. These oscillations correspond to those observed by Zebouni *et al.*[5] in the Hall resistance and magnetoresistance of a cadmium sample. The second set of oscillations was observed only in the Hall effect,[8] at the lowest temperatures. These oscillations will be referred to as short period oscillations since their period is 132 G, or about 4.3 times shorter than the main oscillations.

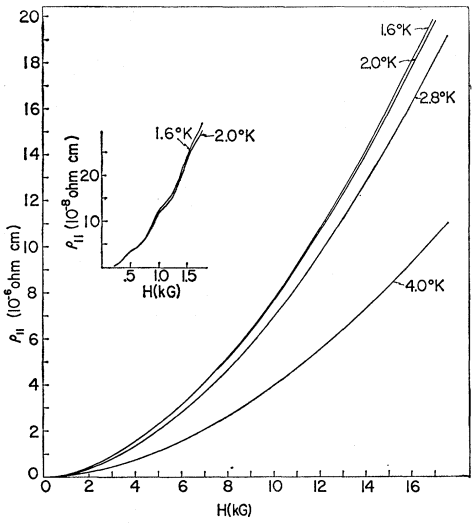

FIG. 3. The transverse magnetoresistivity ρ_{11} plotted as a function of the magnetic field H, for four different temperatures. Low-field size-effect oscillations are shown by the insert for 1.6 and 2.0°K.

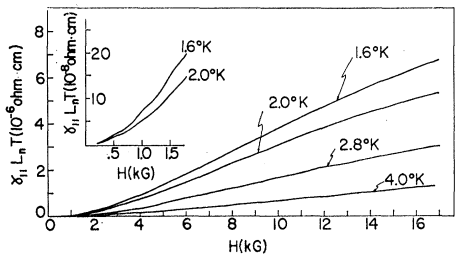

FIG. 4. Transverse thermal magnetoresistivity γ_{11} versus magnetic field H. The value of γ_{11} has been multiplied by the free-electron Wiedemann-Franz ratio L_nT and expressed in (ohm cm), to allow direct comparison with the resistivity data of Fig. 3. Low-field magnetomorphic oscillations are seen in insert for 1.6 and 2.0°K.

Long Period Oscillations

As has already been reported[5,6] these oscillations are believed to be the magnetomorphic oscillations which are expected from the theories of Sondheimer[2] and Blatt.[9] Oscillations in ρ_{11}, γ_{11}, and ϵ_{21}' were very small compared to the gross effects on which they were superposed; therefore they were only visible for small magnetic fields where the gross effect was of the order of the oscillation amplitudes. In the case of ϵ_{21}' it was also necessary to use large heat currents. These quantities are shown in Fig. 3, Fig. 4, and Fig. 5, respectively. Low field oscillations are shown by inserts in each of the figures. Oscillations were much more pronounced in ρ_{21}, γ_{21} and ϵ_{11}' as can be seen in Fig. 6, Fig. 7, and Fig. 8, respectively.

Although the long period oscillations were observed over the entire field range of 400 to 17 000 G in some cases, only oscillations at high field will be considered because they are easier to interpret than the oscillations

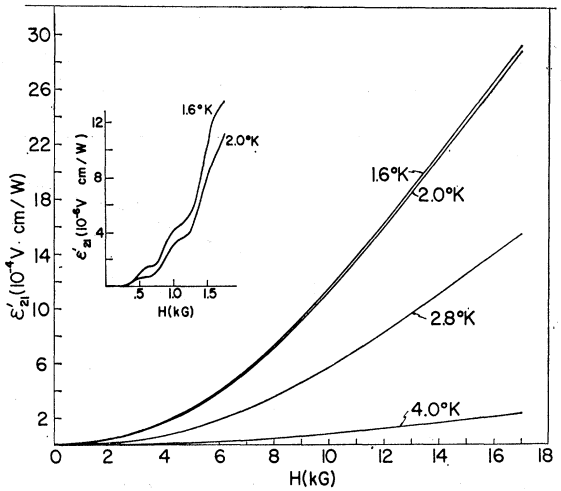

FIG. 5. The adiabatic Nernst-Ettinghausen coefficient ϵ_{21}' showing dependence on magnetic field and temperature. Low-field size-effect oscillations are shown by insert.

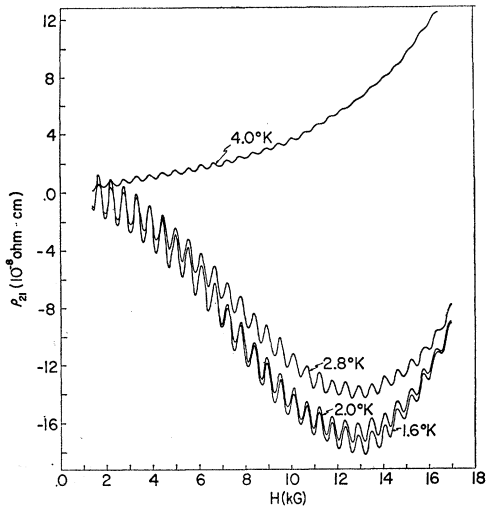

FIG. 6. Hall resistivity ρ_{21} showing magnetomorphic oscillations periodic in the field. Note that the gross effect becomes positive for $T \geq 4.0$°K thus agreeing with the bulk positive Hall effect usually found in cadmium.

occurring at the lower fields. In order to study the oscillations and compare them to theory, the elements of $\hat{\sigma}$, $\hat{\lambda}$, and $\hat{\epsilon}''$ were calculated from the elements of $\hat{\rho}$, $\hat{\gamma}$ and $\hat{\epsilon}'$, using Eq. (3). The corrective term $\hat{\lambda}''-\hat{\lambda}=\hat{\epsilon}''\hat{\pi}$ was found negligible. The elements of the tensors $\hat{\sigma}$, $\hat{\lambda}$ and $\hat{\epsilon}''$ were multiplied by H^n (where n is an appropriate integer) then fitted with a polynomial by the method of least squares, and the gross effect subtracted out to leave only the oscillatory part of the effects. The chosen integers are $n=4$ in the case of σ and λ and $n=3$ in the case of ϵ'' since the theoretical asymptotic quantities $H^4|\tilde{\sigma}|$, $H^4|\tilde{\lambda}''|$ and $H^3|\tilde{\epsilon}''|$ are expected to be constant. The results of such a procedure for $\tilde{\sigma}_{12}$, $\tilde{\lambda}_{12}$, and $\tilde{\epsilon}_{11}''$ at 2.0°K are shown in Figs. 9, 10, 11.

Comparison with Theory

Period. The experimental period of 564±3 G is slightly less than the period expected from the free-electron sphere (572 G), and slightly larger than the period expected for the case of the Ziman lens described above (553 G). There is, then, not much doubt that the lens-shaped electron Fermi surface in the third band is responsible for the long-period morphic oscillations. Trusting the experimental period and the measured sample thickness, one finds that the lens's apex has a radius of curvature $\hbar^{-1}\pi_l = 1.39\pm0.00_7$ Å^{-1} i.e., $r=0.98_6 \pm 0.00_5$ whereas Ziman's lens corresponds to a radius defined by $r=0.96_7$. The discrepancy between the experimental and theoretical value of radius of the lens is not serious and most probably caused from the error which can be made on the correct evaluation of the thickness of the sample. Since the crystal was spark planed, a process which created a thin and irregular polycrystaline layer on the surface, it is possible that the effective value of the thickness a is somewhat smaller than the measured value. Manufacturers of the spark cutter[11] have estimated the depth of damage to lead

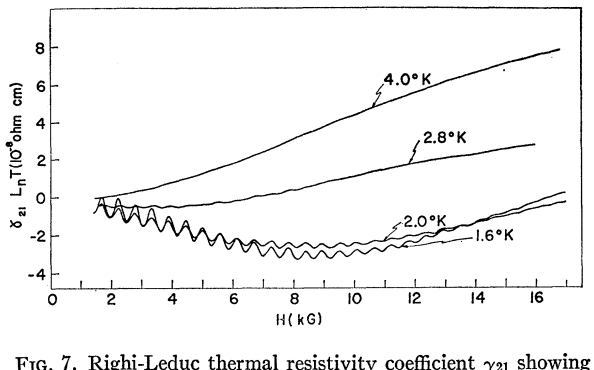

FIG. 7. Righi-Leduc thermal resistivity coefficient γ_{21} showing size-effect oscillations similar to those found in the Hall effect. This effect is multiplied by L_nT for comparison with the ρ_{21} data of Fig. 6.

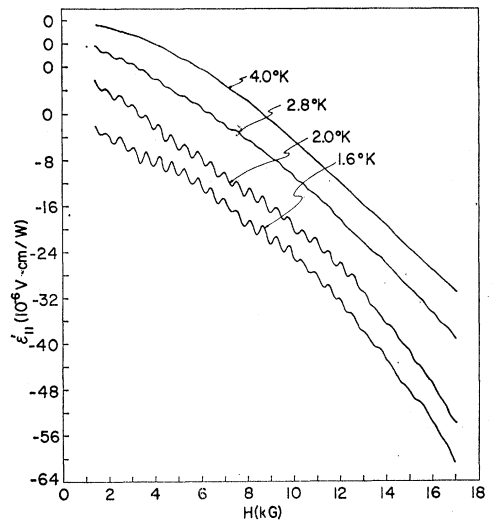

FIG. 8. Size-effect oscillations in the transverse adiabatic thermo-electric coefficient ϵ_{11}'. A different zero position is used for each temperature because of the lack of temperature dependence of this effect.

crystals to be of the order of 25 to 100μ when cut under the same conditions as the cadmium crystal. Thus a slight acid treatment was performed to remove the deteriorated layer. The clear appearance of the etch pattern of an inclusion crystal on the corner of the main crystal was sufficient indication that most of the polycrystaline layer was removed and replaced by the slight irregularities associated with etched surfaces. It is estimated that a 10 microns damaged or irregular layer of the crystal surfaces would be sufficient to bring the r value to agree with the $r=0.96_7$ value expected from the lens model.

Thus it is seen that if this type size-effect oscillation is to be used to make direct measurements of the curvature of the Fermi surface, it is extremely important that the thickness be well known and that the surface damage

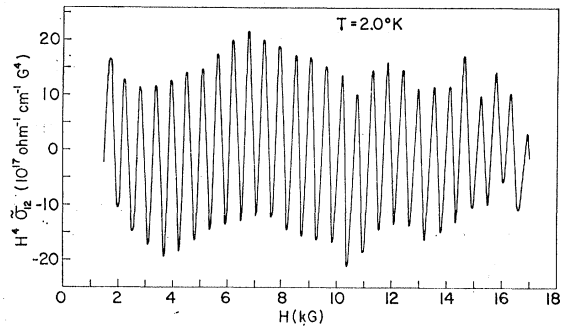

FIG. 9. Oscillatory part of the Hall conductivity σ_{12} (with the gross effect removed) multiplied by H^4 and shown as a function of the field H for 2.0°K.

layer be very small compared to the thickness of the sample. Enlarging the crystal would help but it would also decrease the amplitude of the oscillations exponentially by the factor $e^{-(a/\Lambda)}$, where Λ is the mean free path. Surface damage is reduced by finishing the surface with acid-polishing techniques.

Phase. It has been found that the relative phase of most of the kinetic transport coefficients is in good agreement with theory. A summary of the relative phases of the various effects is as follows:

(a) The oscillations in the quantities $\tilde{\sigma}_{11}$ and $\tilde{\lambda}_{11}$ are found to be in phase. Oscillations in $\tilde{\epsilon}_{12}''$ were too poor for any conclusion to be drawn about their phase.

(b) The oscillations in the quantities $\tilde{\sigma}_{12}$, $\tilde{\lambda}_{12}$, and $\tilde{\epsilon}_{11}''$ are found with a good approximation to be in phase. A lag in phase of $\frac{1}{2}\pi$ exists between these effects and $\tilde{\sigma}_{11}$ as expected from theory in the case of electrons for $\tilde{\sigma}_{12}$ and $\tilde{\lambda}_{12}$, but the phase of $\tilde{\epsilon}_{11}''$ is in disagreement with this expectation.

The absolute phase turns out to be very difficult to determine since the limit of experimental accuracy is reached in trying to make such a determination. In Fig. 12 the field values for the maxima $H_{\max}$ of $\tilde{\sigma}_{12}$ are plotted against the integers. The low-field points should be discarded because a phase shift would appear in the nonasymptotic region, The best straight line through the high-field points in Fig. 12 is given by

$$H_{\max}=(n-\tfrac{1}{8})564\ \text{G}.$$

It is felt that the fact that $\frac{1}{8}$ (i.e., a $\frac{1}{4}\pi$ phase) was

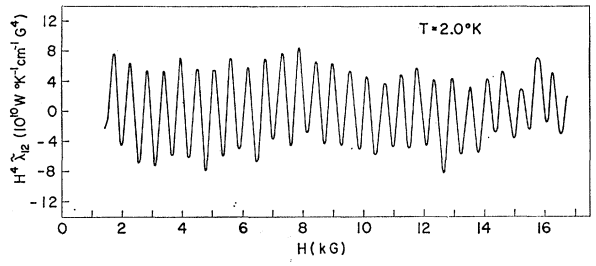

FIG. 10. Oscillatory part of the Righi-Leduc conductivity λ_{12} at 2.0°K multiplied by H^4, as in Fig. 9.

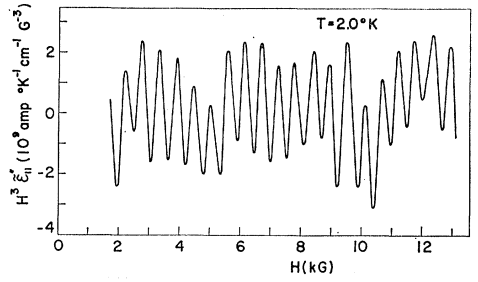

FIG. 11. Oscillatory part of the thermoelectric kinetic coefficient ϵ_{11}'' (2.0°K) multiplied by H^3.

obtained instead of $\frac{1}{4}$ (i.e., a $\frac{1}{2}\pi$ phase) is within experimental error in view of its determination from the far end extrapolation.

Amplitudes. (a) Although the oscillations in $\tilde{\sigma}_{11}$, $\tilde{\lambda}_{11}$ and $\tilde{\epsilon}_{12}''$ were not known with good precision, it was found that $|\tilde{\sigma}_{11}|\approx|\tilde{\sigma}_{12}|$ (this is in agreement with results found by Zebouni, Hamburg and Mackey[5]), that $|\tilde{\lambda}_{11}|\approx|\tilde{\lambda}_{12}|$ and $|\tilde{\epsilon}_{11}''|\approx|\tilde{\epsilon}_{12}''|$. Lack of precision in $\tilde{\sigma}_{11}$, $\tilde{\lambda}_{11}$ and $\tilde{\epsilon}_{12}''$ is attributed to the fact that the gross effect in ρ_{11}, γ_{11}, and ϵ_{21}' was very large compared to the size of the oscillations in those effects. It is felt that the differences of 20% which were actually obtained between $|\tilde{\sigma}_{11}|$ and $|\tilde{\sigma}_{12}|$ are within experimental error and that the theoretical prediction $|\tilde{\sigma}_{11}|=|\tilde{\sigma}_{12}|$ is satisfactorily demonstrated. For the same reasons, it is felt that the experiments are also in good agreement with the predictions $|\tilde{\lambda}_{11}|=|\tilde{\lambda}_{12}|$ and $|\tilde{\epsilon}_{11}''|=|\tilde{\epsilon}_{12}''|$. In the remainder of this paper the equality is assumed to hold for the effects discussed above and only the results of the most precisely known of the oscillations are used. For example, Figs. 13, 14, and 15 show the averaged peak to peak amplitudes $2H^4|\tilde{\sigma}_{12}|$, $2H^4L_nT|\tilde{\lambda}_{12}|$ and $2H^3|\tilde{\epsilon}_{11}''|$ as functions of the field for several temperatures.

(b) Comparison of Figs. 13 and 14 shows that good agreement with the Wiedemann-Franz law is obtained for the magnitudes of the oscillations. Inspection of Eq. (7b) shows that for $K'>K$ (which is expected since mean free paths for thermal processes are shorter than

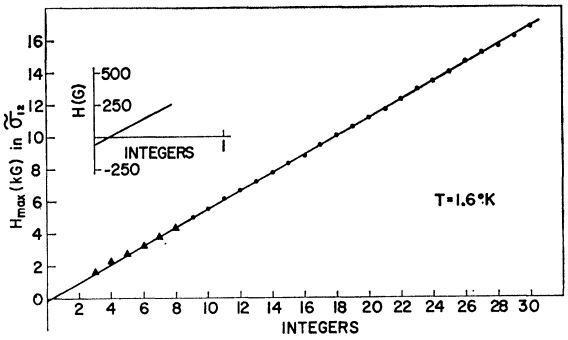

FIG. 12. Field positions of the maxima of the oscillations in σ_{12} plotted against integers. The slope of the line gives the experimental period (565 G) while the intercept is related to the absolute phase. Insert shows that the intercept is of the order of −70 G.

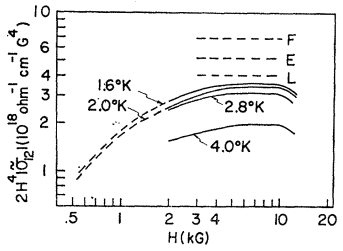

FIG. 13. Averaged amplitude of the oscillations in the quantity $2H^4\tilde{\sigma}_{12}$ shown as a function of field H. The amplitude of the oscillations in $\tilde{\sigma}_{12}$ are seen to fall off as H^{-4} in the range 4 to 11 kG. E, F, L represent respectively, the experimental extrapolated value, the free-electron expected value, and the lens-shaped surface expected value.

mean free paths for electrical processes) the amplitudes of the oscillations in the thermal conductivity and Righi-Leduc effect should be smaller than those in the electrical conductivity and the Hall effect.

(c) Examination of Figs. 9, 10, 13 and 14 shows that the amplitudes of $\tilde{\sigma}_{12}$ and $\tilde{\lambda}_{12}$ fall off as H^{-4} for fields between 4 to 10 kG and then fall off more rapidly at higher fields. The H^{-4} dependence in $\tilde{\sigma}_{12}$ is in agreement with results found by Hamburg and Zebouni.[15] Similarly, Figs. 11 and 15 show that $\tilde{\epsilon}_{11}''$ falls off as H^{-3} for the region 4 to 10 kG and then falls off more rapidly at higher fields. No explanation is offered for the field dependence of the effects below 4 kG since this not considered to be the asymptotic region. The fact that the oscillation amplitudes do not follow the H^{-4} dependence above 11 kG is believed to be due to the fact that the crystal faces were not perfectly plane and parallel. There is no way of ascertaining the depth and variation of the damage to the surface caused by spark cutting and the subsequent etching irregularities. Thus the over-all effective thickness would vary from point to point in a range $a\pm\Delta a$ which would create a dispersion in the period by an amount $P\pm\Delta P$, and thus tend to decrease the amplitude of the oscillations corresponding to large integers. About 20 oscillations are observed before such dispersive effects become noticeable and by

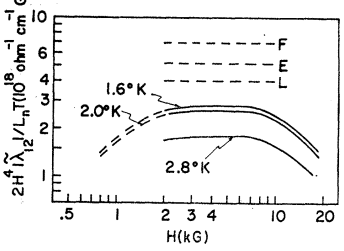

FIG. 14. Averaged amplitudes of the oscillations in the quantity $2H^4(L_nT)^{-1}\tilde{\lambda}_{12}$ shown as a function of field. Comparison with Fig. 13 shows that $(L_nT)^{-1}\tilde{\lambda}_{12}$ has approximately the same amplitude and field dependence as $\tilde{\sigma}_{12}$.

[15] R. Hamburg, Master's thesis, Louisiana State University, 1964 (unpublished).

the time 30 oscillations have been observed, the amplitude of the oscillations has dropped to about 60% of its expected value. It is in qualitative agreement with an order of magnitude for $\Delta a/a$ of about 1%, i.e., the irregularities in the depth of the damaged layer should be expected to be about 10μ.

(d) It can be noted that the experimental amplitude of $\tilde{\sigma}_{12}$ and $\tilde{\lambda}_{12}$ corresponding to the flat region of the curves in Figs. 13 and 14 are only slightly less than the amplitudes predicted for the free-electron sphere and the Ziman lens, which are indicated by the letters F and L, respectively. This agreement corroborates the identification of the lens as the cause of the morphic oscillation. More precise comparison can be done if an experimental evaluation of the quantities e^{-K} can be made or if the extrapolation of the amplitude $|\tilde{\sigma}_{12}|$ and $|\tilde{\lambda}_{12}|$ to the case of infinite mean free path ($e^{-K}=1$) is effected. Such an extrapolation as outlined in the last chapter and on Fig. 18 leads to a value $H^4|2\tilde{\sigma}_{12\infty}|=5\times10^{18}\Omega^{-1}$ cm^{-1} G^4 and is indicated in Fig. 13, Fig. 14 and Fig. 18 by the letter E. The agreement with the theory can be seen to be excellent.

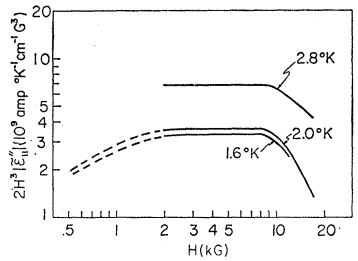

FIG. 15. Averaged amplitudes of the oscillations in the quantity $2H^3\tilde{\epsilon}_{11}''$ shown as a function of field. $|\tilde{\epsilon}_{11}''|$ is seen to fall off as H^{-3} in about the same region as $|\tilde{\sigma}_{12}|$ and $|\tilde{\lambda}_{12}|$ fall off as H^{-4}.

The same cannot be said for comparison of the experimental and theoretical amplitudes of the thermoelectric oscillations: here the experimentally obtained oscillations are about 20 times larger than expected. Since the experimental values of $\tilde{\epsilon}_{11}''$ are determined by an involved tensor calculation, it might be thought that accumulated errors on the experimental coefficient ρ, γ, and ϵ' could generate values of $\tilde{\epsilon}_{11}''$ abnormally large and of the wrong phase. To eliminate any doubt about this question an entirely new set of experiments was performed and the calculations made again. The results were almost identical with the results of the first set of experiments. This seems to eliminate the possibility that the discrepancy was caused by the incidence in the tensor calculation of some experimental errors. Another possibility might have been that the thermoelectric power of the constantan leads was not corrected for the calculations. This possibility was discarded when it was found that the term which would have contained the thermoelectric power of the leads was not of the proper phase and magnitude to explain the oscillations found in $\tilde{\epsilon}_{11}''$. Assuming all possibilities of experimental errors

have been eliminated, it can be stated that the $\tilde{\epsilon}''$ results are anomalous with respect to free electron theory and to the case of the lens. Indeed, matching the experimental data to Eq. (19) leads to $r=0.98_6$ and $(1-\nu)^{-2}(\partial\pi_z/\partial p_z)^{-2}=0.79_3$, i.e., a fair agreement, but trying to match also Eq. (20) leads to $(m^*/m_0)(\partial\pi_z/\partial p_z)=33$ a result which is incompatible with cadmium band structure. Therefore, the anomalous amplitude in the ϵ_{11}'' morphic oscillation remains still unexplained. Rough estimates from other possible causes which may influence the ϵ_{11}'' data such as phonon drag does not seem to account for the anomaly either.

Short-Period Oscillations

These oscillations were first detected when it was found that what appeared to be an unexplained noise in the measurement of the oscillations in ρ_{21} was entirely reproducible at 1.6°K. By lowering the temperature to 1.3°K and adjusting the amplifier system to optimum values, it was found that the "noise" was a set of oscillations periodic in the field[8] superposed on the main set of long-period oscillations. Figure 16 shows a section of the recorder trace with the two sets of oscillations drawn in and the noise removed. Up to 70 of the short period oscillations were observed. A detailed study of these oscillations would be difficult because of their small amplitude. However, a check of the orientational dependence indicates that the relative amplitude of the small period oscillations to the long period oscillations is nearly independent of the field direction for angles between the field and hexagonal axis of the crystal of up to 10 deg. The ratio of amplitudes found was $|\tilde{\rho}_{21}|_{\text{long}}/|\tilde{\rho}_{21}|_{\text{short}}\approx 10$. The periods of the long and short oscillations are very insensitive to orientation in this range. A check of 43 of the short period oscillations showed that the period of the oscillations was practically constant with the ratio of long to short oscillations being given by $P_{\text{long}}/P_{\text{short}}=4.3$.

Since these size-effect oscillations are expected to be due to sections of the Fermi surface where dS_z/dp_z has an extremum, the lack of orientational dependence of the period indicates that the Fermi surface is one of a type where the extremum of dS_z/dp_z is relatively constant over angles of about 10 deg. This is, for example, the case of the extremal values near the apex of the lens-shaped surface of cadmium used in the interpretation of the long period oscillation. Examination of published information[12,16] on the Fermi surface suggests that perhaps the "hole arms" in the second Brillouin zone might be responsible for the short oscillations (see Fig. 17). The maximal extremum which exists on one of the arms could cause the oscillation; however, it is not obvious that dS_z/dp_z would be constant enough with respect to orientation changes to account for the experimental results, but as pointed out later the truncation effect due to the branching of the arm would provide for an effect more insensitive to orientation.

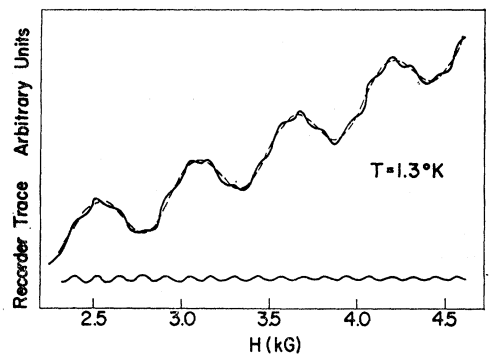

FIG. 16. The top curve represents a recorder trace for the oscillations in ρ_{21} (Hall resistivity) which show the short-period oscillations (132 G) superimposed on the long-period oscillations (565 G). The separate contribution of those short-period oscillations are shown on the lower curve.

If these oscillations are assumed to be due to the hole arms then the present results could be compared to the findings of Daniel and MacKinnon[12] (DM). In their study of magnetoacoustic absorption in cadmium made with the magnetic field and the direction of motion of the longitudinal sound waves in the hexagonal direction an oscillatory field dependence of the attenuation coefficient was interpreted as corresponding to the extremal value of $\partial S_z/\partial p_z$ of the hole arms.

If it is required that the distance traveled in the z direction in one orbit around the Fermi surface,[12] i.e.,

$$\oint v_z dt=-\frac{c}{eH}\frac{\partial S_z}{\partial p_z}$$

should be some submultiple of the thickness of the crystal, then

$$\frac{a}{n}=-\frac{c}{eH_n}\frac{\partial S}{\partial p_z} \quad \text{or} \quad \frac{\partial S}{\partial p_z}=\frac{ea}{c}P,$$

where n is an integer and $H_n/n=P$ the period of the oscillations when $\partial S_z/\partial p_z$ corresponds to an extremum or to a singularity. The short oscillation period of $P=132$ G corresponds to $\hbar^{-1}(\partial S_z/\partial p_z)=2.04$ Å^{-1}. The result quoted by DM of $\hbar^{-1}(\partial S/\partial p_z)=0.68$ Å^{-1} attributed to the hole arms, can be seen to be exactly three times smaller than that presently obtained from the short period oscillation. The apparent discrepancy with DM results seems to indicate that the branching of the arms suggested by Harrison[16] and illustrated by Gibbons and Falicov[17] and Grassie[18] would be correct.

As pointed out at the end of the theoretical section, magnetomorphic oscillation would appear whenever $(\partial S_z/\partial p_z)$ reaches some extremal value or presents singularities. The singular property of the holes arm

[16] W. A. Harrison, Phys. Rev. **118**, 1190 (1960).
[17] D. F. Gibbons and L. M. Falicov, Phil. Mag. **8**, 177 (1963).
[18] A. D. C. Grassie, Phil. Mag. **9**, 847 (1964).

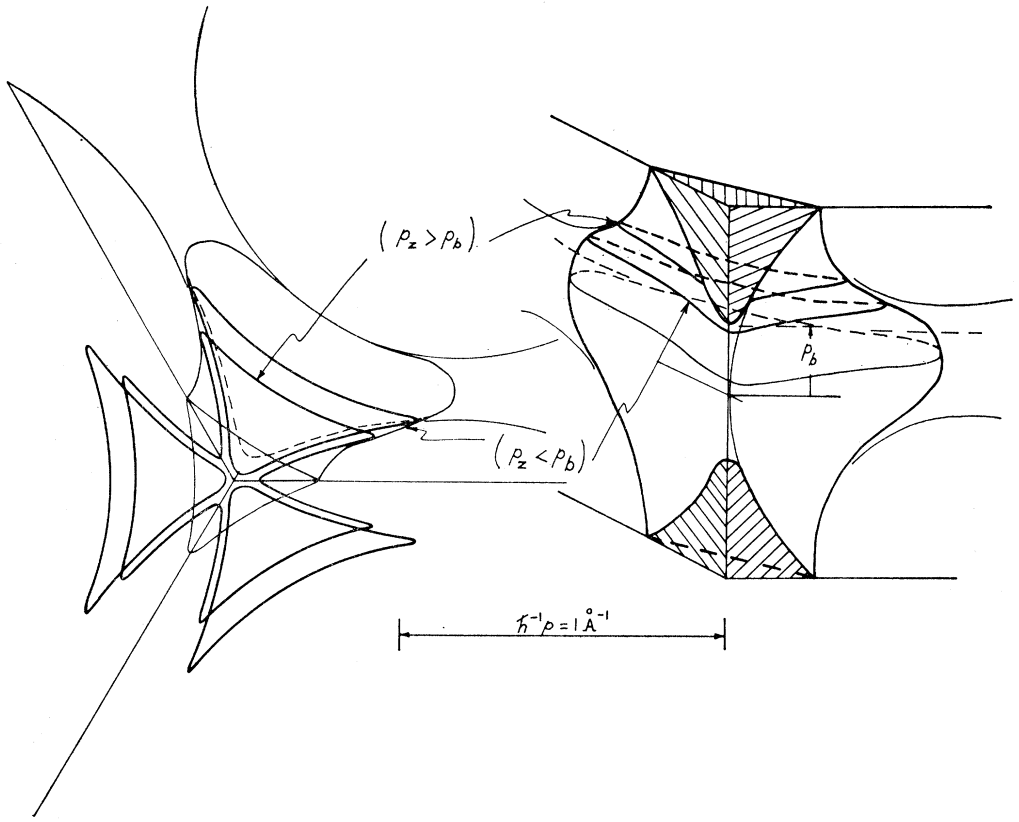

FIG. 17. The right side of the figure is an approximative representation of part of the "hole" Fermi surface in the second zone. The left side of the figure shows cross sections of this hole surface in the repeated zone representation for two values of p_z, $\hbar^{-1}p_z=0.18$ Å^{-1} and $\hbar^{-1}p_z=0.27$ Å^{-1}. They characterize the shape of the electron orbits when slight deformations from the free-electron case are taken into consideration. In one case ($\hbar^{-1}p_z=0.18$ Å^{-1}) the orbit takes place around one branch of the hole surface; in the other case ($\hbar^{-1}p_z=0.27$ Å^{-1}) it takes place around the set of three adjacent merging branches.

which may be stressed is the fact that, built up along an edge of the zone adjacent to two other zones, it splits into three branches[16–18] at a level here referred to as p_b (see Fig. 17). The truncation of the arm at $p_z=p_b$ is characterized by the discontinuity $S(p_z=p_b^+)=3S(p_z=p_b^-)$ in the Fermi surface cross section, with approximately $[\partial S(p_b^+)/\partial p_z]\approx 3[\partial S(p_b^-)/\partial p_z]$. This last relation would explain the two values of 2.04 Å^{-1} and 0.68 Å^{-1} obtained from the two different experimental methods. Acoustic resonance would be sensitive to the smaller value of $(\partial S/\partial p_z)$, i.e., corresponding to orbit around one branch and obtained for p_b^-, whereas a galvanomorphic effect would be sensitive to the larger value of $(\partial S/\partial p_z)$ corresponding to the orbit around the unsplit arm for p_b^+. The two types of orbits are illustrated in Fig. 17. The free-electron approximation for this part of the Fermi surface would have the arm remaining in contact all the way along the vertical edge of the zone. However, any small overlap of the Fermi surface due to an energy gap would immediately create suitable conditions for such splitting of the arm into three branches. The value of $\hbar^{-1}(\partial S_z/\partial p_z)$ can be computed for the free-electron approximation and is equal to 2.04 Å^{-1} for $\hbar^{-1}p^z=0.202$ Å^{-1}. The deformation from the free-electron approximation would most probably be such that $\hbar^{-1}p_b<0.202$ Å^{-1}. Since $(\partial S/\partial p_z)=0$ for $p_z=0$ there will be two values of p_z, p_{b1} and p_{b2} corresponding to $\hbar^{-1}(\partial S_z/\partial p_z)=2.04$ Å^{-1} and with an intermediate value p_m $(p_{b1}>p_m>p_{b2})$ for which $(\partial S_z/\partial p_z)$ would pass through a maximum value $|\partial S_z/\partial p_z|_m$. (It could be possible that $|\partial S_z/\partial p_z|_m$ would be very close to the 2.04 Å^{-1} value; such possibility would largely enhance the corresponding morphic oscillations.) The expected asymptotic behavior for the amplitude in $\tilde{\sigma}_{12}$ in the case of truncated type of singularity is a H^{-3} field dependence, as compared to the H^{-4} behavior of the long-period oscillations. It should be expected thus that the short-period oscillations in ρ_{21} would show an increase in amplitude with the field and as compared with the amplitude of the long-period oscillations. The fact that this behavior is not observed would simply be related to the dispersive effect due to the surface imperfection and the associate decay of the amplitude with the increase in the oscillation integer number which for the short period oscillations is more than four times that for the long-period oscillations.

Some Considerations About the Bulk Effects and Gross Size Effects

In the galvanomagnetic effects

$$\hat{\sigma}=(\bar{\sigma}_{11}+i\bar{\sigma}_{12})+(\tilde{\sigma}_{11}+i\tilde{\sigma}_{12}),$$

the gross effect $\bar{\sigma}_{11}+i\bar{\sigma}_{12}$ is known with sufficient precision whenever easily separated from the oscillatory component $\tilde{\sigma}_{11}+i\tilde{\sigma}_{12}$, a condition which requires a large enough field and for which the transport equations simplify to their asymptotic limit.[13] Taking the nonoscillatory term out of Eq. (12), it can be shown that the lens contribution to conductivity is $\bar{\sigma}_{11}+i\bar{\sigma}_{12}=\hat{\sigma}_b\{1-\alpha^{-1}(\pi_z)_{\rm av}\}$ where $\hat{\sigma}_b$ is the bulk contribution $\hat{\sigma}_b=e^2\int a\alpha^{-1}dn_z$, where the integration is carried over the volume of the lens, and where dn_z is the number of electrons in the slice p_z, p_z+dp_z of the lens. If it is supposed that $\pi_z/v_z=m^*$ is independent of p_z as in the case of Ziman's lens, then

$$a^{-1}\alpha=\frac{1}{\tau}\frac{\pi_z}{v_z}+i\frac{eH}{c}\frac{e}{c}=-(H_l+iH)=-H_l'$$

is independent of p_z and $\hat{\sigma}_b=ecN_lH_l'^{-1}$ will be the lens contribution to bulk conductivity, with N_l number of electrons in the lens and $H_l=cm_l^*/e\tau$.

With the same assumption as above, $(\pi_z)_{\rm Av}$ is the average $(1/N_l)\int\pi_z dn_z$ and a good approximation in the lens case as in the quadratic case would be $(\pi_z)_{\rm Av}\approx(3/8)\pi_l$.

With P_j the morphic period due to the band j and defining $H_{sj}=(3/8)(P_j/2\pi)$, then

$$\bar{\sigma}_{11}+i\bar{\sigma}_{12}=ec\sum N_jH_j'^{-1}(1-H_{sj}H_j'^{-1}) \qquad (21)$$

if all band j can be assimilated to lens shaped or quadratic (with axial symmetry) Fermi surfaces. Here $H_j'=(H_j\pm iH)$ with the upper and lower signs corresponding to electrons and holes, respectively.

For high fields $H\gg H_j$[13] the transverse conductivity and Hall conductivity take the simple form

$$H^2\bar{\sigma}_{11}=ec\sum N_j(H_j+H_{sj}), \qquad (22a)$$

$$H\bar{\sigma}_{12}=ec\sum\pm N_j\{1-H_j(H_j+2H_{sj})H^{-2}\}. \qquad (22b)$$

Identical expressions would be obtained for the electronic part of the thermal conductivity in the form of $(L_nT)^{-1}\lambda_e''$ except for larger values of the H_j. The corresponding expressions for thermoelectric effect can be obtained starting from the nonoscillatory part of Eq. (12) or more simply by applying the relation $\hat{\epsilon}''=(\pi^2k^2T/3e)(\partial\hat{\sigma}/\partial\mathcal{E})$ $(\mathcal{E}=\zeta)$ which is found valid in the magnetomorphic case and in which $\hat{\sigma}$ is given by Eq. (21). The asymptotic condition yields

$$H\bar{\epsilon}_{12}''=-(\pi^2k^2cT/3)\sum Z_j \qquad (23a)$$

$$H^2\bar{\epsilon}_{11}''=(\pi^2k^2cT/3)\sum\pm Z_j(H_j+\tfrac{4}{3}H_{sj}+\tfrac{2}{3}\mu_jH_j) \qquad (23b)$$

if all band j can be assimilated to lens-shaped or quadratic, axially symmetric Fermi surfaces. The index j refers to all bands; $j=l$ for the lens. In the two-band model $j=e$ and $j=h$ would be used for electrons and holes, respectively. The index s is, as defined, to characterize the size effect. In further computation all H_{sj} will be neglected except H_{sl} of the lens ($H_{sl}=33.8$ G). The bulk time of relaxation is supposed energy-dependent with the law $\tau=\mathcal{E}^\mu$ and as can be seen in Eqs. (22) and (23) only $\bar{\epsilon}_{11}''$ is affected by this energy dependence.

A certain number of parameters in the Eqs. (22) and (23) can be determined from the comparison with the experimental result.

Mean-Free-Path Determination

The bulk time of relaxation τ appears in $\bar{\sigma}_{11}$ through the saturation fields $H_j=cm_j^*/e\tau$. Should $1/\tau$ tend to zero the asymptotic value $H^2\bar{\sigma}_{11}$ would tend to the size part $ec\sum N_jH_{sj}\approx ecN_lH_{sl}$.

The bulk time of relaxation also appears in the asymptotic amplitude of the morphic oscillation through the term e^{-K}. Defining $\tilde{\sigma}_{12\infty}$ the Hall-conductivity-oscillation values extrapolated to the condition of infinite mean free path, then $e^{-K}=\tilde{\sigma}_{12}/\tilde{\sigma}_{12\infty}$ and

$$K=\ln 2H^4|\tilde{\sigma}_{12\infty}|-\ln 2H^4|\tilde{\sigma}_{12}|$$
$$=\beta(H^2\bar{\sigma}_{11}-ecN_lH_{sl}). \qquad (24)$$

Those relations should hold also when the σ terms are replaced by the corresponding $\lambda_e(L_nT)^{-1}$ terms. In the semi-log representation in Fig. 18 of $2H^4|\tilde{\sigma}_{12}|$ versus $H^2\bar{\sigma}_{11}$ for different temperature and field values, a linear

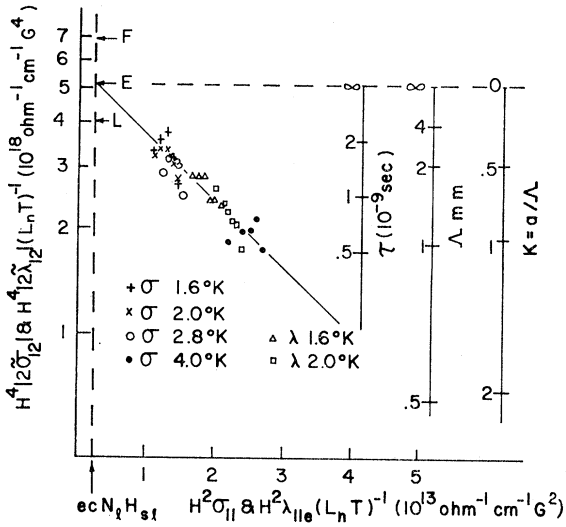

FIG. 18. Variation of the amplitude in the magnetomorphic oscillations $|\tilde{\sigma}_{12}|$ and $|\tilde{\lambda}_{12}|$ as a function of the time of relaxation τ, the time of relaxation being supposed to be proportional to the gross $\bar{\sigma}_{11}$ or $\tilde{\lambda}_{11e}$ conductivity. The $\ln H^4|2\tilde{\sigma}_{12}|$ values are seen to be linearly depending on $H^2\bar{\sigma}_{11}$, with the mean free path infinite or $K=0$ for $H^2\sigma_{11}\approx ecN_lH_{sl}$. The K scale, the mean-free-path scale, and the time of relaxation scale are thus determined and shown on the right side of the figure. The different points, for different field values correspond to σ data (+ at 1.6°K, × at 2.1°K, ○ at 2.8°K, ● at 4°K) and to λ data (△ at 1.6°K, □ at 2.1°K).

TABLE I. Parameters related to the mobility of the electrons and phonons.

Temperature °K	I Λ_σ mm	II Λ_λ mm	III τ_σ 10^{-9} sec	IV τ_λ 10^{-9} sec	V $H_{l\sigma}$ G	VI $H_{l\lambda}$ G	VII α_b	VIII α	IX λ_g 10^{-2} W°K^{-1} cm^{-1}	X Λ_g micron
1.6	3.0	1.8	1.9	1.2	30	47	0.63	0.68	0.30_5	2.0
2.0	2.5	1.3	1.6	0.8	35	70	0.5	0.6	0.51_5	1.7
2.8	2.0		1.3		44				1.3	1.6
4.0	1.2		0.75		76			0.22	3.1_5	1.3

dependence of $\ln 2H^4|\bar{\sigma}_{12}|$ is achieved and it is seen that $2H^4|\bar{\sigma}_{12}|$ extrapolates to the value $2H^4|\bar{\sigma}_{12\infty}| \approx 5\times10^{18}$ (Ω^{-1} cm^{1-} G^4) for $H^2\bar{\sigma}_{11} \approx ecN_lH_{sl} = 2.4\times10^{11}$ (Ω^{-1} cm^{-1} G^2) (N_l is approximated from calliper size to be $N_l \approx 4.4\times10^{21}$ cm^{-3}). This extrapolated value is represented in Figs. 13, 14, and 18 by the letter E. This value corresponds to $e^{-K}=1$, i.e., $K=0$ or $\Lambda=\infty$; scales for both K and Λ (the electron bulk mean free path) can be determined and are shown on the right side of Fig. 18. A direct mean-free-path reading can be made by use of the Λ scale, and despite a slight field variation, average values for Λ_σ can be obtained for each temperature and are shown in Table I, column I. The index σ refers to mean free paths corresponding to the galvanomagnetic effect. It may be seen that the mean free paths are in the millimeter range. When the electronic thermal conductivity λ_e terms are used in Eq. (24) and plotted on Fig. 18, mean free paths corresponding to the thermal process Λ_λ can also be determined and are given in Table I, column II. The ratio $\alpha_b=\Lambda_\lambda/\Lambda_\sigma$ or bulk scattering efficiency shown in Table I, column VII is a measurement of how efficient is the scattering in galvanic process as compared to thermal process. The fact that α_b is close to unity at the lowest temperature indicates that impurity scattering is already preponderant. It may be estimated that impurity-scattering mean free paths at 0°K would be of the order of 5 mm. The ratio $\alpha=\bar{\lambda}_{11e}/(\bar{\sigma}_{11}L_nT)$ given in Table I, column VIII is, at high field, a measurement of the apparent efficiency which differs from α_b the bulk efficiency, since the size scattering is also included. As expected, α is larger than α_b.

Columns III and IV of Table I give the values of the bulk time of relaxation $\tau=\Lambda/v_F$ where the Fermi velocity[12] v_F is taken as 1.58×10^8 cm/sec. A τ scale is also shown in Fig. 18. Since the lens cyclotron mass m_l^* is practically equal to the free-electron mass, the saturation field $H_l=cm_l^*/e\tau$ for the lens would be the same as that for a free electron $H_l=H_0=cm_0/e\tau$ and these values at the different temperatures are given in Table I, columns V and VI for electrical processes (σ) and thermal processes (λ), respectively.

Lattice Thermal Conductivity and Phonon Mean Free Path

With the thermal conductivity given by $\hat{\lambda}=\hat{\lambda}_e+\hat{\lambda}_g$ the lattice contribution λ_g can in principle be separated as the curve λ_{11} versus σ_{11} extrapolates to the value λ_g when $\sigma_{11}\to0$. The λ_g values thus obtained are shown in Table I, column IX and seem to decrease with temperature following approximately the law $\lambda\sim T^{2.45}$. A phonon-size effect scattering would give a T^3 law and a phonon-electron normal scattering a T^2 law; the experimental result would suggest an intermediate situation. Nevertheless, it would be more correct to suggest the preponderance of the electron-phonon process (normal process plus a remnant of umklapp process), since the phonon mean free paths Λ_g are too small compared to the sample size. An order of magnitude of Λ_g can be obtained with $\Lambda_g=3\lambda_g(C_gv_g)^{-1}$ where the lattice specific heat C_g is calculated with a Debye temperature $\theta=172$°K and the sound velocity v_g[12] is taken as 3800 m/sec. The phonon mean free paths are seen in Table I, column X to be within micron range.

The Electrical Conductivity, the Carrier Densities, and the Magnetic Breakdown

Equation (22a) predicts that $\bar{\sigma}_{11}$ depends linearly on H^{-2} and tends to zero as $H\to\infty$. Experimentally the linear dependence is achieved but the extrapolation $H\to\infty$ gives a $\bar{\sigma}_{11\infty}$ value slightly different from zero. Should any weight be given to this behavior it may be suggested that it is due to a small fraction $\delta N'$ of open orbit carriers. If those carriers are attributed a mass m_0 and the relaxation time τ_σ of Table I, the values $\delta N'$ are found to be of the order of 10^{-16} e cm^{-3} or 10^{-7} e atom^{-1} as can be seen in Table II column I. It may be suggested that at high fields a few electrons may be filtering through the pinched off region of the hole ring as well as filtering from one arm branch to another near the lateral edge of the zone, i.e., a weak reminiscence of the occurrence in zinc and magnesium of the magnetic break-down of the hole ring.[10,19] But some ambiguity exists between the temperature dependence of $\delta N'$ and the preceding interpretation.

When $H^2\bar{\sigma}_{11}$ is corrected from the $H^2\bar{\sigma}_{11\infty}$ and ecN_lH_{sl} terms, an estimated value of $\sum N_jH_j$ can be obtained. In Table I, column IV the normalized value $N'=H_{l\sigma}^{-1}\times\sum N_jH_j$ is given. It can be considered to be a good approximation for the total number of carriers supposing that most carriers have masses nearly equal to m_0.

Although a fairly good analysis of $\bar{\sigma}_{11}$ can be made, it is not the same for $\bar{\sigma}_{12}$. Firstly, the expected condition $\sum\pm N_j=0$ is not achieved and only a simple analysis

TABLE II. Parameters "independent" of the temperature and related to the carriers density and density of states. As a means of comparison the free-electron sphere would have an electron density of $N_0=9.46\times10^{22}$ e cm^{-3} and a density of state $Z_0=1.16\times10^{34}$ e cm^{-3} erg^{-1}. Estimated values for the lens-shaped Fermi surfaces in the third zone are $N_l\approx0.44\times10^{22}$ e cm^{-3} and $Z_l\approx0.2\times10^{34}$ e cm^{-3} erg^{-1}.

Temperature °K	I $\delta N'$	II ΔN_σ (10^{16} e cm^{-3})	III ΔN_λ	IV N' (12^{22} e cm^{-3})	V $\Delta N''$	VI Z^{eff}	VII Z_c (10^{34} e cm^{-3} erg^{-1})	VIII $\Delta Z'$
1.6	1.2_4	~160	~200	1.8		$1\,6_5$	1.2_2	~−25
2.0	1.6			1.7		1.8_8	1.2_2	~−28
2.8	2.			1.6		2.0_4	1.0	~−22
4.0	4.2	−95	−5000	1.7	0.38	1.3_5	0.45	~−30

with $\sum\pm N_j=\Delta N_\sigma$ constant, can be made at 4.0°K. The ΔN_σ values are shown in column II of Table II with excess of holes at 4.0°K and excess of electrons at other temperatures, but in this latter case the ΔN_σ would be highly field-dependent, reminiscent of one magnetic breakdown oscillation in zinc.[10] The term $ec\sum\mp N_jH_j\times(H_j+2H_{sj})H^{-2}$ is only a fraction of the $H\bar{\sigma}_{12}$ data. At 4°K, for example, the normalized value $\Delta N'=H_l^{-2}\times[\sum\pm N_jH_j(H_j+2H_{lj})]$ given in Table I column V agrees with a two-band model in which $N_e=N_h=N'/2$, $H_e\approx H_l$ and $H_h\approx H_l/2$, that is to say the electrons with mass m_0 and holes with mass$\approx0.5m_0$. The analysis of $\bar{\lambda}_{11e}$ gives agreement within experimental error with the conclusion from the $\bar{\sigma}_{11}$ analysis, but the analysis of $\bar{\lambda}_{12}$ adds some confusion to the conclusion obtained from the $\bar{\sigma}_{12}$ data as can be seen for ΔN_λ in column III of Table II.

Thermoelectric Coefficients and Density of States

As expected from Eq. (23a) the Nernst-Ettinghausen term $H\bar{\epsilon}_{12}''$ is nearly field-independent and the effective density of states $Z^{\text{eff}}=\sum Z_j$ can be obtained and seen in Table II, column VI to be slightly larger than the free electron estimated value of 1.16 e cm^{-3} erg^{-1} and slightly temperature-dependent. Some partial phonon drag may explain this behavior. If an estimated value of full phonon drag is made[20] and full phonon drag supposed to exist in the Cd crystal, the electronic density of state Z_c would be obtained by dividing the Z^{eff} values of Table II, column VI by a coefficient of order of $(1+0.135T^2)$ and the resulting value Z_c shown in column VII of Table II indicates that taking account of a full phonon drag leads to an over-correction at the upper temperatures. The $H^2\bar{\epsilon}_{11}''$ values expected from Eq. (23b) should be field-independent. This is found to be a poor approximation. The order of magnitude of the normalized quantity $\Delta Z'=H_{l\sigma}^{-1}\sum\pm Z_j[H_j+\frac{2}{3}\mu_jH_j+\frac{4}{3}H_{sj}]$ is indicated in Table II, column VIII. They are an order of magnitude larger than expected when compared to Z^{eff}; it may be an indication that the H_j would be larger than the $H_{j\sigma}$; it may also have some bearing on the unexplained large amplitude found in the $\bar{\epsilon}_{11}''$ magnetomorphic oscillation; but the most probable cause of the large monotonic $\bar{\epsilon}_{11}''$ value would be associated to the thermocouple effect due to the constantan leads $(-\sigma_{11}\epsilon_{\text{ctn}})$. Indeed, a reasonable ϵ_{ctn} value, nearly field-independent, $\epsilon_{\text{ctn}}\approx+0.45T$ μV(°K)$^{-1}$ would generate this $\bar{\epsilon}_{11}''$ apparently large value.

CONCLUSION

Periods, phases and amplitudes of the long-period magnetomorphic oscillations in the transport coefficients are in relatively good agreement with free-electron theory with the exception of $|\bar{\epsilon}_{11}''|$ and $|\bar{\epsilon}_{12}''|$, which are an order of magnitude too large. Regardless of the discrepancy in $|\bar{\epsilon}''|$, it is felt that the relatively good fit of the rest of the results to free-electron theory indicates that the lens-shaped Fermi surface in the third Brillouin zone of cadmium is responsible for the oscillations. Extension of the theory to the case of lens-shaped Fermi surfaces confirms this identification, but still fails to account for the large oscillations in $|\bar{\epsilon}''|$. Magnetomorphic oscillations of the type studied arise whenever the surface derivative $\partial S_z/\partial p_z$ has an extremum or a singularity. Such an extremum is attained at the lens apex and the corresponding period leads to the determination of the radius of curvature π_l of the lens at this apex; π_l is found to be about 98% the value of the free-electron sphere radius.

There is no Fermi-surface apex (in the hexagonal direction) which could cause the appearance of morphic oscillations with the short period found for the second set of oscillations. But an extremum value for $\partial S_z/\partial p_z$ of the right order of magnitude is expected in the hole arm of the second zone if this arm is in contact with the arms in the adjacent zones. More likely, and to be in agreement with Daniel and MacKinnon's results, the cause of the short-period oscillation is the singularity (discontinuity) of $\partial S_z/\partial p_z$ at the point the hole arm starts to make contact with the two adjacent arms.

If attempts are made to use magnetomorphic oscillations to study Fermi surfaces, it is important that the crystal faces be plane, parallel, undamaged, and that a very accurate determination of the effective thickness be made. The Hall effect has been found the most sensitive of the transport coefficients for the study of the magnetomorphic oscillations.

The gross behavior of the transport effect is generally well accounted for, except for the case of Hall and

[19] R. W. Stark, T. G. Eck, W. L. Gordon, and F. Moazed, Phys. Rev. Letters 8, 360 (1962).

[20] J. R. Long, C. G. Grenier, and J. M. Reynolds, Phys. Rev. **140**, 187 (1965).

Righi-Leduc effects. The gross value of the thermoelectric coefficient $\bar{\epsilon}_{11}''$ is found to be an order of magnitude too large as it also appears in its oscillatory component.

ACKNOWLEDGMENTS

The authors wish to express their appreciation to Dr. N. H. Zebouni for his interest and cooperation, and to Dr. G. Hussey for reading the manuscript. The authors are also indebted to Dr. G. N. Rao, Dr. H. J. Mackey and Dr. J. R. Long for assistance in the various phases of the research. Thanks are extended to the members of the Low Temperature Group, most particularly to C. R. Crosby and R. E. Hamburg for helping in some phases of the work.

PHYSICAL REVIEW VOLUME 143, NUMBER 2 MARCH 1966

Low-Temperature Specific Heats of α-Phase Copper-Silver Alloys

G. A. SARGENT, L. L. ISAACS,* AND T. B. MASSALSKI
Mellon Institute, Pittsburgh, Pennsylvania
(Received 11 October 1965)

Heat-capacity measurements between 1.6 and 4.2°K were made on a series of α-phase copper-silver alloys. The results suggest that the density of states at the Fermi surface decreases slightly upon alloying. Values of the effective thermal mass calculated from the data are also found to decrease upon alloying. These results are interpreted to mean that the Fermi surface is becoming more spherical.

INTRODUCTION

INTEREST in the electronic structure of the noble-metal alloy phases has been stimulated by the experimental determination of the topography of the Fermi surface in copper, silver, and gold.[1] By means of new techniques, it has been demonstrated that in these metals the Fermi surface is already in contact with the {111} faces of the Brillouin zone. The degree of contact appears to be smallest in the case of silver, so that its Fermi surface resembles most closely the free-electron sphere with slight distortions in the [111] directions.

From the above observations, it follows, in terms of simple models of the band structure,[2] that the density of states at the Fermi level should *decrease* initially upon alloying the noble metals with elements whose addition increases the electron concentration, e.g., *B*-subgroup elements.

Unfortunately, the techniques used to determine the topography of the Fermi surface in the pure metals, for example the measurement of the de Haas–van Alphen effect, cannot be used in the case of alloys unless they are highly ordered.[3] This is because the increased scattering caused by randomly introduced solute atoms substantially reduces the mean free path of the conduction electrons. However, it is well recognized that the measurement of electronic specific heat yields a direct measure of the density of states at the Fermi level, and hence this technique can be used to probe the band structure of dilute alloy systems. The experiments of Rayne, on the α phases of the copper-zinc[4,5] and copper-germanium[6] systems have shown an increase in the electronic component of the specific heat upon alloying. A similar trend is also found in silver-tin[7,8] and silver-cadmium[9] alloys, and these results which indicate an increase in the density of states are difficult to explain in terms of a simple model of the band structure of the noble metals. In a recent attempt to reconcile experimental observations and theory, Jones[10] has pointed out that on alloying the broadening of the Fermi level caused by the impurity scattering is large when compared with the thermal broadening in the pure metals at low temperatures. Such scattering should produce a virtual contribution to the electronic specific heat particularly if the details of the band structure in the vicinity of the Fermi level include sharp changes in the density of states as is the case in copper, silver, and gold where it is known that a peak in the density of states exists just below the Fermi level. This proposed contribution should be observable even when the electron concentration and the band structure remains unchanged on alloying.

The work described in the present paper was designed

* Present address: Argonne National Laboratory, Argonne, Illinois.

[1] *The Fermi Surface*, edited by W. A. Harrison and M. B. Webb (John Wiley & Sons, Inc., New York, 1960).
[2] J. M. Ziman, Advan. Phys. **10**, 1 (1961).
[3] A. Beck, J. P. Jan, W. B. Pearson, and I. M. Templeton, Phil. Mag. **8**, 351 (1963).
[4] J. A. Rayne, Phys. Rev. **108**, 22 (1957).
[5] B. W. Veal and J. A. Rayne, Phys. Rev. **128**, 551 (1962).
[6] J. A. Rayne, Phys. Rev. **110**, 606 (1958).
[7] B. A. Green, Jr. and H. V. Culbert, Phys. Rev. **137**, A1168 (1965).
[8] T. B. Massalski and L. L. Isaacs, Phys. Rev. **139**, A138 (1965).
[9] H. Montgomery and G. P. Pells, Conference on The Electronic Structure of Alloys, University of Sheffield, 1963 (unpublished).
[10] H. Jones, Phys. Rev. **134**, A958 (1964).